Title	The Damage analysis for irradiation tolerant spin-driven thermoelectric device based on single-crystalline $Y_3Fe_5O_{12}$/Pt heterostructures
Author(s)	Ieda Junichi, Okayasu Satoru, Harii Kazuya, Kobata Masaaki, Yoshii Kenji, Fukuda Tatsuo, Ishida Masahiko, Saito Eiji
Citation	IEEE Transactions on Magnetics, 58(8), p.1301106_1-1301106_6
Text Version	Accepted Manuscript
URL	https://jopss.jaea.go.jp/search/servlet/search?5072880
DOI	https://doi.org/10.1109/TMAG.2022.3145888
Right	IEEE

The damage analysis for irradiation tolerant spin-driven thermoelectric device based on single-crystalline $Y_3Fe_5O_{12}$/Pt heterostructures

Jun'ichi Ieda[1], Satoru Okayasu[1], Kazuya Harii[2], Masaaki Kobata[3], Kenji Yoshii[3], Tatsuo Fukuda[3], Masahiko Ishida[4], and Eiji Saitoh[1,5,6,7]

[1]Advanced Science Research Center, Japan Atomic Energy Agency, Tokai, Ibaraki 319-1195, Japan.

[2]Department of Functional Materials Research, National Institutes for Quantum Science and Technology, Takasaki 370-1292, Japan.

[3]Materials Sciences Research Center, Japan Atomic Energy Agency, Hyogo 679-5148, Japan.

[4]System Platform Research Laboratories, NEC Corporation, Kawasaki 211-8666, Japan.

[5]Department of Applied Physics, The University of Tokyo, Tokyo 113-8656, Japan

[6]WPI Advanced Institute for Materials Research, Tohoku University, 980-8577, Japan

[7]Center for Spintronics Research Network, Tohoku University, Sendai 980-8577, Japan

Abstract

Spin-driven thermoelectric (STE) generation based on the combination of the spin Seebeck effect and inverse spin Hall effect is an alternative to conventional semiconductor-based thermocouples as it is large-scale, low-cost, and environment-friendly. The STE device is thought to be radiation hard, making it attractive for space and nuclear technology applications. By using magnetometry, transmission electron microscopy, and the hard X-ray photoemission spectroscopy (HAXPES) measurements, we show that an STE device made of single-crystalline $Y_3Fe_5O_{12}$/Pt heterostructures has tolerance to irradiation of high-energy heavy ion beams. We used 200 MeV gold ion beams modeling cumulative damages due to fission products emitted from the surface of spent nuclear fuels. By varying the dose level, we confirmed that the thermoelectric and magnetic properties of the single-crystalline $Y_3Fe_5O_{12}$/Pt STE device are finite at the ion-irradiation dose up to 10^{12} ions/cm^2 fluence. In addition, the HAXPES measurements were performed to understand the effects at the interface of $Y_3Fe_5O_{12}$/Pt. The HAXPES data suggest that the chemical reaction regarding Fe and O that diminishes the SSE signals is promoted with the increase of the irradiation dose. The understandings of the damage analysis in $Y_3Fe_5O_{12}$/Pt are beneficial for developing better STE devices applicable to harsh environmental usages.

I. INTRODUCTION

There is great potential for the development of thermoelectric generators [1] that operate in harsh environments such as space exploration and nuclear facilities. In fact, the Mars rover that was launched recently is powered by a radioisotope thermoelectric generator (RTG) [2]. A thermoelectric element that converts heat into electricity usually uses thermocouples in which different semiconductors are connected. However, this structure is vulnerable to high-energy radiation and causes performance deterioration. For this reason, the radioisotopes as a heat source that make up the RTGs are limited to a few nuclear species (^{238}Pu in practice) emitting only alpha particles that can be easily shielded. In order to overcome this restriction, it is necessary to introduce a new concept thermoelectric conversion technology. For this purpose, we focus on spintronics that harnesses the electron spin in solids. Spintronics is highly expected as an energy-saving technology in the field of information and communication devices [3,4]. In addition to this excellent energy-saving property, spintronic devices are proved to be resistant to radioactive irradiation [5-7], which causes fatal damages in semiconductor-based devices, and spintronics-based memory devices are equipped at logic circuits of artificial satellites and flight computers of aircraft that are routinely exposed to high irradiation. Especially, a spin-driven thermoelectric (STE) generation based on the combination of the spin Seebeck effect (SSE) [8-10] and inverse spin Hall effect (ISHE) [11,12] is a promising as it can be large-scale, low-cost, and environment-friendly. The SSE refers to the generation of spin current along with the temperature gradient in ferromagnetic materials and the ISHE converts the induced spin current to the transverse electromotive force via spin orbit interactions in heavy metals.

The semiconductor-free STE devices are thought to be radiation hard. So far, the radiation resistance of the STE devices has been tested by irradiating them with high-energy gamma (γ) ray [13] and heavy-ion beams [14] where the STE performance was maintained over the dose levels up to 3×10^5 Gy of γ rays and 10^{10} ions/cm^2 fluence of 320 MeV gold ion (Au^{24+}) beams respectively. Moreover, for ion irradiation, the maximum dose level was determined as about 10^{12} ions/cm^2 fluence where the columnar defects caused by the ion tracks entirely amorphized the ferromagnetic layer of the STE device. In the previous report [14], we used STE samples that consist of a metallic layer Pt and a ferromagnetic insulator $Y_3Fe_5O_{12}$ (YIG) fabricated by the metal-organic decomposition (MOD) method [15]. The method creates a columnar YIG crystal structure aligned perpendicular to the film plane that offers quasi-one-dimensional spin conducting paths. Since the YIG films prepared by the MOD method contain a lot of voids outside the columnar structure ion-irradiation tolerance of the STE devices can be different when a single-crystalline YIG is used.

To discuss the effect of porosity in YIG used in the previous study we complement, in the present work, the damage analysis against high-energy heavy-ion irradiation for the STE device using single-crystalline YIG/Pt heterostructures based on magnetization, SSE, and hard X-ray photoemission spectroscopy (HAXPES) measurements. We also discuss amorphization of the crystal structure created by the ion tracks in the YIG/Pt heterostructure based on transmission electron microscope (TEM) images. These observations supplement the irradiation tolerance performance and degradation mechanism of the STE device in general.

II. EXPERIMENTAL AND DISCUSSION

The STE sample for the present study was fabricated by sputtering single-crystalline YIG (100 nm thickness) on a gallium garnet ($Gd_3Ga_5O_{12}$, GGG) substrate (500 μm thickness). After air annealing the substrate (825°C for 3 min 20 sec in air), the Pt layer was deposited with 5nm thicknesses on the surface of YIG. For the thermoelectric voltage measurements, the sample was cut into small chips. We confirmed that the sample exhibited the typical SSE output signals.

Next, we performed ion irradiation on the samples with varying the dose level. One sample was set aside as a reference. High energy ion beams were produced at the Tandem accelerator in Japan Atomic Energy Agency Tokai laboratory. We used gold ions (Au^{+24}) accelerated to the energy 200 MeV that were irradiated on the samples from the Pt side as shown in Fig. 1a at room temperature. Due to a high energy heavy ion passing through the samples high-density electrons are excited and columnar defects are formed along the ion tracks [16-18] (Fig.1b). Typical TEM images of the irradiated samples are shown in Fig.1c. There are columnar defects created in the single crystalline YIG layer. Within the columnar defects, the crystal structure is randomized due to the rapid heating and cooling process associated with the electron excitations along the ion tracks [19-23]. Note that it was hard to observe the ion tracks in the MOD-made YIG/Pt samples [14]. It is found that the hillocks of the amorphized YIG were formed at the YIG/Pt interface as observed at the surface of YIG samples [23]. These columnar defects and hillocks are amorphous regions with ~13 nm and 14 nm in diameter respectively, which is consistent with the previous report [24]. On the other hand, the Pt layer and its surface were not affected by the ion irradiation because of the quick diffusion of transferred energy

from ions by electrons in the metal. This result contrasts to the case of ion-implantation with much lower energy (several keV) where the ions accumulate near the sample surface leading to enhancement of spin relaxation [25]. Since the length of the track that depends on the ion energy is calculated as approximately 15 μm for 200 MeV Au ions, ions irradiated from the Pt side penetrate both the Pt and YIG layers and end within the GGG substrate (Fig.1a). Since amorphous YIG is paramagnetic and does not contribute to the spin transport at room temperature [26], the irradiated regions become ineffective for thermoelectric energy conversion via the SSE.

Using the irradiated samples, we evaluate the thermoelectric conversion property of the single crystalline YIG/Pt systems. Figure 2a shows a change of the SSE voltage as functions of applied magnetic fields H with the fixed applied temperature ΔT = 8 K and the Au ion fluence, Φ, varying in the range of $\Phi = 0–1.0\times10^{13}$ ions/cm^2. The measurement setup for the SSE is schematically shown in Fig. 2b. The spin current induced along the applied temperature difference ΔT between Pt and the substrate. The spin current injected into the Pt layer is then converted into an electromotive force by the ISHE in the direction orthogonal to both the magnetization and heat current directions. The gap between electrodes for the ISHE voltage measurement is 3 mm. The SSE voltage decreases with the ion fluence, and entirely disappears above the dose of $\Phi = 1\times10^{13}$ ions/cm^2. The linearity of the SSE voltages with ΔT is maintained for all as-irradiated samples suggesting that the decrease of the SSE voltage is a result of an increase of the damaged (amorphized) area of the sample.

As we reported in Ref. [14], the decrease of SSE signals during the ion irradiation process is mainly due to the change of the magnetization of the YIG layer. Figure 2c shows hysteresis loops of

the irradiated samples exhibiting a change of the magnetization with the ion fluence. The behavior exhibits a similar trend as that of the SSE voltage signals. The fluence dependence of the SSE coefficient and the saturation magnetization *M* are summarized in Fig.2d. The fitting curve for *M* in Fig. 2d is calculated by the coverage model considering overlapping of ion track [27] as

$$M(\Phi) = M(\Phi = 0) \times (1 - \exp(-\pi r^2 \Phi)),$$

where Φ is the ion beam fluence, *r* is the average radius of the ion tracks. From the fitting, we obtained *r* = 6.2 nm, which is consistent with the diameter estimated from the TEM image (~13 nm) shown in Fig. 1c. This plausibly suggests that the decrease of the SSE signal is mainly due to the change of magnetization.

When we compare the present results with the MOD-based YIG/Pt case [14] we observe that the reduction of the SSE voltage and magnetization from as-prepared sample to that irradiated at low dose level ($\Phi = 1\times10^{11}$ ions/cm^2) becomes rather prominent as shown in Fig. 2d. This implies that the single-crystalline YIG is more susceptible to the crystalline damage caused by the ion tracks than the MOD-based YIG with many voids that can absorb the stress. It should be also noted that the magnetization remains finite at the highest dose level $\Phi = 1\times10^{13}$ ions/cm^2 where the columnar defects are expected to cover the entire surface of the sample. The possible origin of this observation is the recrystallization of a heavily irradiated YIG crystal reported at a similar dose level [20]. The recrystallization process recovers the bulk magnetization while the damage accumulated at the YIG/Pt interface that is critical to the degradation of SSE conversion efficiency cannot be restored.

To investigate the damage accumulated at the YIG/Pt interface the HAXPES measurements

were carried out using synchrotron radiation at the beamline BL22XU of SPring-8 [28]. Since this method offers large probing depths of photoelectrons up to several nanometers with the aid of x-ray energies typically above 5 keV, it has been known as a powerful tool for non-destructive measurements of true bulk states and buried interface [29-31]. The incident X-ray energy for the present study was 8 keV. The total energy resolution was approximately 300meV. The various photoelectron peaks such as Fe $2p_{3/2}$, O 1*s*, Pt 4*f*, and Y $2p_{3/2}$ were measured at room temperature. The other experimental details have been noted elsewhere [32]. Figures 3a-d shows respectively HAXPES spectra in the Pt 4*f*, Y $2p_{3/2}$, O 1*s*, and Fe $2p_{3/2}$ regions for various dose levels. The spectral intensity is normalized to the Pt 4*f* spectral intensity obtained from the same sample. The binding energies of Pt 4*f* and Y $2p_{3/2}$ do not change (Fig.3a, b) whereas those of O 1*s* shift monotonically to larger values with the increase in the irradiation dose (Fig.3c), suggesting an occurrence of interfacial chemical reaction [14]. In addition, the spectral intensity of O 1*s* is gradually suppressed. This behavior suggests that oxygen atoms are desorbed at YIG/Pt interfaces, which is likely the origin of the chemical reaction. The small peak in the higher binding energy for as-irradiated samples may be related to the oxygen deficiency. The shift of binding energy and the suppression of peak intensity were also found for Fe $2p_{3/2}$ (Fig.3d). Hence, the interfacial reaction is plausibly triggered by the deficiency of Fe as well as O. The small increase in the peak intensity of Y $2p_{3/2}$ with the irradiation dose (Fig.3b) also supports this scenario by thinking as the relative raise compared to the decreases in those of O 1*s* and Fe $2p_{3/2}$. The Fe deficiency seems to be consistent with the segregation of metallic Fe at the surface of Pt film, as discussed earlier [32].

III. CONCLUSION

In summary, we investigated the ion-irradiation effects on the STE device consisting of single-crystalline YIG/Pt heterostructures. The 200 MeV Au ions were used to simulate the device damage caused by high-energy fission products from radioisotopes that are equipped to a RTG unit as a heat source. The general trends that the SSE voltages are reduced as the magnetization decreases due to the amorphization caused by the ion tracks was confirmed in the present study. As compared with that of the MOD-based YIG/Pt heterostructures studied previously, the reduction of the SSE voltage and magnetization is more susceptible in the dose level $\Phi = 1\times10^{11}$ ions/cm^2 while they remain finite at the fluence $\Phi = 1\times10^{12}$ ions/cm^2 where the signals had vanished previously [14]. Moreover, the magnetization became finite with vanishing SSE signal at the dose level $\Phi = 1\times10^{13}$ ions/cm^2 where the ion tracks were estimated to cover the whole surface. We consider that these behaviors can be ascribed to the damage accumulated in the bulk crystalline structure and restored magnetization by the recrystallization process that was studied extensively in Ref. [20]. Based on the comparison between the present results and those in Ref. [14], the effect of porosity in the YIG made in MOD method can be concluded to be favorable in absorbing the stress caused by the irradiation damage. As for the damage accumulated at the YIG/Pt interface the HAXPES measurement revealed the chemical reaction regarding Fe and O were promoted by the ion irradiation. All these results supplement our knowledge regarding the irradiation tolerance of the STE devices that is still very limited.

ACKNOWLEGEMENTS

The authors thank T. Hioki for sample preparation and T. Taguchi, C. Suzuki, and S. Yamamoto for assistance in taking the TEM images. This work was supported by JST-ERATO “Spin Quantum Rectification Project” (Grant No. JPMJER1402), Innovative Nuclear Research and Development Program (JPMXD0212345678), and JSPS KAKENHI (Grant Nos. JP17K05126, JP17K19090, JP19H05600, and JP21H04643). The ion irradiation experiments were performed at the tandem accelerator with the approval of Proposal No. 2018SP03. The synchrotron radiation experiments were performed at the BL22XU of SPring-8 with the approval of the Japan Synchrotron Radiation Research Institute (JASRI) (Proposal Nos. 2017A3731, 2019A3731, 2019B3731, and 2020A3731).

REFERENCES

[1] H. J. Goldsmid, *Introduction to Thermoelectricity* (Springer, 2010).

[2] https://mars.nasa.gov/internal_resources/788/

[3] B. Dieny *et al.*, "Opportunities and challenges for spintronics in the microelectronics industry," *Nat. Electron.* **3**, 446 (2020); doi: 10.1038/s41928-020-0461-5

[4] A. Hirohata *et al.*, "Review on spintronics: Principles and device applications," *J. Magn. Magn. Mater.* **509**, 166711 (2020); doi: 10.1016/j.jmmm.2020.166711.

[5] D. Kobayashi *et al.*, "Influence of Heavy Ion Irradiation on Perpendicular-Anisotropy CoFeB-MgO Magnetic Tunnel Junctions," *IEEE Trans. Nucl. Sci.* **61**, 1710 (2014); doi: 10.1109/TNS.2014.2304738.

[6] B. C. Pursley *et al.*, "Robustness of n-GaAs carrier spin properties to 5 MeV proton irradiation," *Appl. Phys. Lett.* **106**, 072403 (2015); doi: 10.1063/1.4907286.

[7] E. A. Montoya *et al.*, "Immunity of nanoscale magnetic tunnel junctions with perpendicular magnetic anisotropy to ionizing radiation," *Sci. Rep.* **10**, 10220 (2020); doi: 10.1038/s41598-020-67257-2.

[8] K. Uchida *et al.*, "Observation of the spin-Seebeck effect," *Nature* **455**, 778–781 (2008); doi:10.1038/nature07321.

[9] K. Uchida *et al.*, "Spin Seebeck insulator," *Nat. Mater.* **9**, 894 (2010); doi: 10.1038/NMAT2856.

[10] K. Uchida *et al.*, "Thermoelectric Generation Based on Spin Seebeck Effects," *Proc. IEEE*

104, 1946 (2016); doi: 10.1109/JPROC.2016.2535167.

[11] E. Saitoh, M Ueda, H. Miyajima, and G. Tatara, "Conversion of spin current into charge current at room temperature: Inverse spin-Hall effect," *Appl. Phys. Lett.* **88**, 182509 (2006); doi: 10.1063/1.2199473.

[12] K. Ando *et al.*, "Inverse spin-Hall effect induced by spin pumping in metallic system," *J. Appl. Phys.* **109**, 103913 (2011); doi: 10.1063/1.3587173.

[13] A. Yagmur *et al.*, "Gamma radiation resistance of spin Seebeck devices," *Appl. Phys. Lett.* **109**, 243902 (2016); doi: 10.1063/1.4971976.

[14] S. Okayasu *et al.*, "Tolerance of spin-Seebeck thermoelectricity against irradiation by swift heavy ions," *J. Appl. Phys.* **128**, 083902 (2020); doi: 10.1063/5.0014229.

[15] A. Kirihara *et al.*, "Spin-current-driven thermoelectric coating," *Nat. Mater.* **11**, 686 (2012); doi: 10.1038/nmat3360.

[16] A. Meftah, F. Brisard, J. M. Costantini, M. Hage-Ali, J. P. Stoquert, F. Studer, and M. Toulemonde, "Swift heavy ions in magnetic insulators: A damage-cross-section velocity effect," *Phys. Rev. B* **48**, 920 (1993); doi: 10.1103/PhysRevB.48.920.

[17] J. Jensen, A. Dunlop, S. Della-Negra, and M. Toulemonde, "A comparison between tracks created by high energy mono-atomic and cluster ions in $Y_3Fe_5O_{12}$," *Nucl. Instrum. Methods Phys. Res. B* **146**, 412 (1998); doi: 10.1016/S0168-583X(98)00442-X.

[18] J. M. Costantini, F. Brisard, L. Autissier, M. Caput, and F. Ravel, "Study of the amorphization of ion-irradiated yttrium iron garnet by high-resolution diffraction techniques," *J. Phys. D:*

Appl. Phys. **26**, A57 (1993); doi: 10.1088/0022-3727/26/4A/013.

[19] J. M. Costantini, J. M. Desvignes, A. Pérez, and F. Studer, "Local order and magnetic behavior of amorphous and nanocrystalline yttrium iron garnet produced by swift heavy ion irradiations," *J. Appl. Phys.* **87**, 1899 (2000) ; doi: 10.1063/1.372110.

[20] J. M. Costantini, J. M. Desvignes, and M. Toulemonde, "Amorphization and recrystallization of yttrium iron garnet under swift heavy ion beams," *J. Appl. Phys.* **87**, 4164 (2000); doi: 10.1063/1.373047.

[21] J. M. Costantini, F. Studer, and J. C. Peuzin, "Modifications of the magnetic properties of ferrites by swift heavy ion irradiations," *J. Appl. Phys*. **90**, 126 (2001); doi: 10.1063/1.1365056.

[22] J. M. Costantini, S. Miro, F. Beuneu, and M. Toulemonde, "Swift heavy ion-beam induced amorphization and recrystallization of yttrium iron garnet," *J. Phys.: Condens. Matter* **27**, 496001 (2015); doi: 10.1088/0953-8984/27/49/496001.

[23] N. Ishikawa, T. Taguchi, and N. Okubo, *Nanotechnology* **28**, 445708 (2017); doi: 10.1088/1361-6528/aa8778.

[24] N. Ishikawa, T. Taguchi, A. Kitamura, G. Szenes, M. E. Toimil-Molares, and C. Trautmann, *J. Appl. Phys.* **127**, 055902 (2020); doi: 10.1063/1.5128973.

[25] I. Barsukov *et al.*, "Frequency dependence of spin relaxation in periodic systems," *Phys. Rev. B* **84,** 140410(R) (2011); doi: 10.1103/PhysRevB.84.140410.

[26] J. M. Gomez-Perez *et al.*, "Absence of evidence of spin transport through amorphous

$Y_3Fe_5O_{12}$," *Appl. Phys. Lett.* **116**, 032401 (2020); doi: 10.1063/1.5119911.

[27] G. Fuchs, F. Studer, E. Balanzat, D. Groult, J. C. Jousset, and B. Raveau, "High energy heavy ion irradiation effects in yttrium iron garnet," *Nucl. Instrum. Methods Phys. Res. B* **12,** 471 (1985); doi: 10.1016/0168-583X(85)90502-6.

[28] M. Kobata *et al.*, *JPS Conference Proceedings* **30**, 011192 (2020); doi: 10.7566/JPSCP.30.011192.

[29] E. Ikenaga *et al.,* "Interface reaction of poly-Si/high-k insulator systems studied by hard X-ray photoemission spectroscopy," *J. Electron Spectrosc. Relat. Phenom.* **144-147**, 491 (2005); doi: 10.1016/j.elspec.2005.01.180.

[30] C. Zborowski *et al.*, "Quantitative determination of elemental diffusion from deeply buried layers by photoelectron spectroscopy," *J. Appl. Phys.* **124**, 085115 (2018); doi: 10.1063/1.5033453.

[31] G. Conti *et al.*, "Characterization of free-standing InAs quantum membranes by standing wave hard x-ray photoemission spectroscopy," *APL Mater.* **6**, 058101 (2018); doi: 10.1063/1.5022379.

[32] M. Kobata *et al.*, "Chemical form analysis of reaction products in Cs-adsorption on stainless steel by means of HAXPES and SEM/EDX," *J. Nucl. Mater.* **498**, 387 (2018); doi: 10.1016/j.jnucmat.2017.10.035.

Figure captions

Fig. 1. The STE device for the present study. (a) The STE device structure that consists of a metallic layer Pt (5 nm thickness), a ferromagnetic insulator $Y_3Fe_5O_{12}$ (YIG) single crystal layer (100 μm thickness), and a $Gd_3Ga_5O_{12}$ (GGG) substrate (500 μm thickness). The heavy ion beam (solid arrows) irradiated from the Pt side penetrates the Pt and YIG layers and ends within the GGG substrate with forming ion tracks represented by dashed lines. (b) The schematic side view of the YIG/Pt heterostructure. At the position indicated by the solid arrows, the ion tracks are formed with capping by the hillocks, which are amorphous YIG. (c) Bright field image of the single crystalline YIG irradiated with 200 MeV Au at vertical incidence to the YIG/Pt interface. The black solid lines corresponding to the boundary between the crystalline and amorphous regions are guides for the eye.

Fig. 2. Measured SSE voltage and magnetization for the ion-irradiated samples with the fluence, Φ = 0, 1×10^{11}, 1×10^{12}, 1×10^{13} ions/cm^2. (a) The output voltage signals as a function of applied magnetic fields H from -100 to 100 mT. The temperature difference ΔT between Pt and the substrate is fixed as ΔT= 8 K. (b) The schematic view of measurement setup for the SSE output voltage. The SSE voltage is detected from the contacts attached to the Pt layer in the direction perpendicular to both the magnetization along the applied magnetic field and the spin current along with the temperature difference. (c) The magnetization vs applied magnetic fields from -100 to 100 mT for the irradiated samples. (d) The fluence dependence of the SSE coefficient defined by the SSE voltage per temperature difference, VSSE/ΔT (filled circles) and saturation magnetization (filled squares). The

solid curve represents the calculated coverage ratio of the sample surface by the ion tracks.

Fig. 3. HAXPES spectra of the single-crystalline YIG/Pt heterostructure samples for various dose levels in the (a) Pt 4*f*, (b) Y $2p_{3/2}$, (c) O 1*s*, and (d) Fe $2p_{3/2}$ regions.

Figure 1

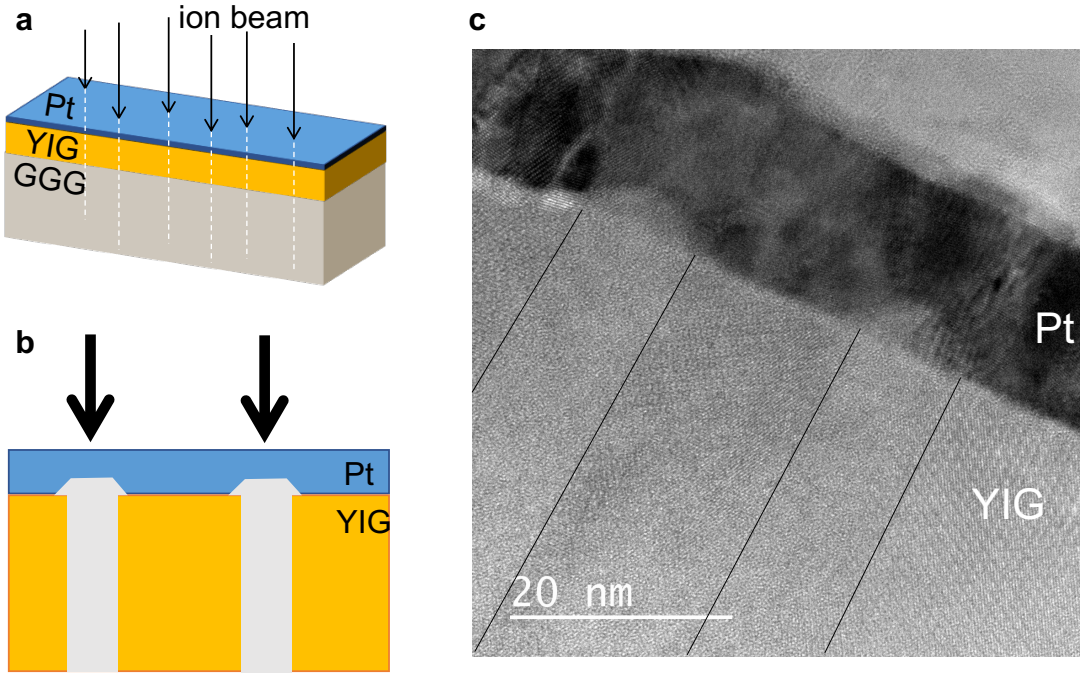

Figure 2

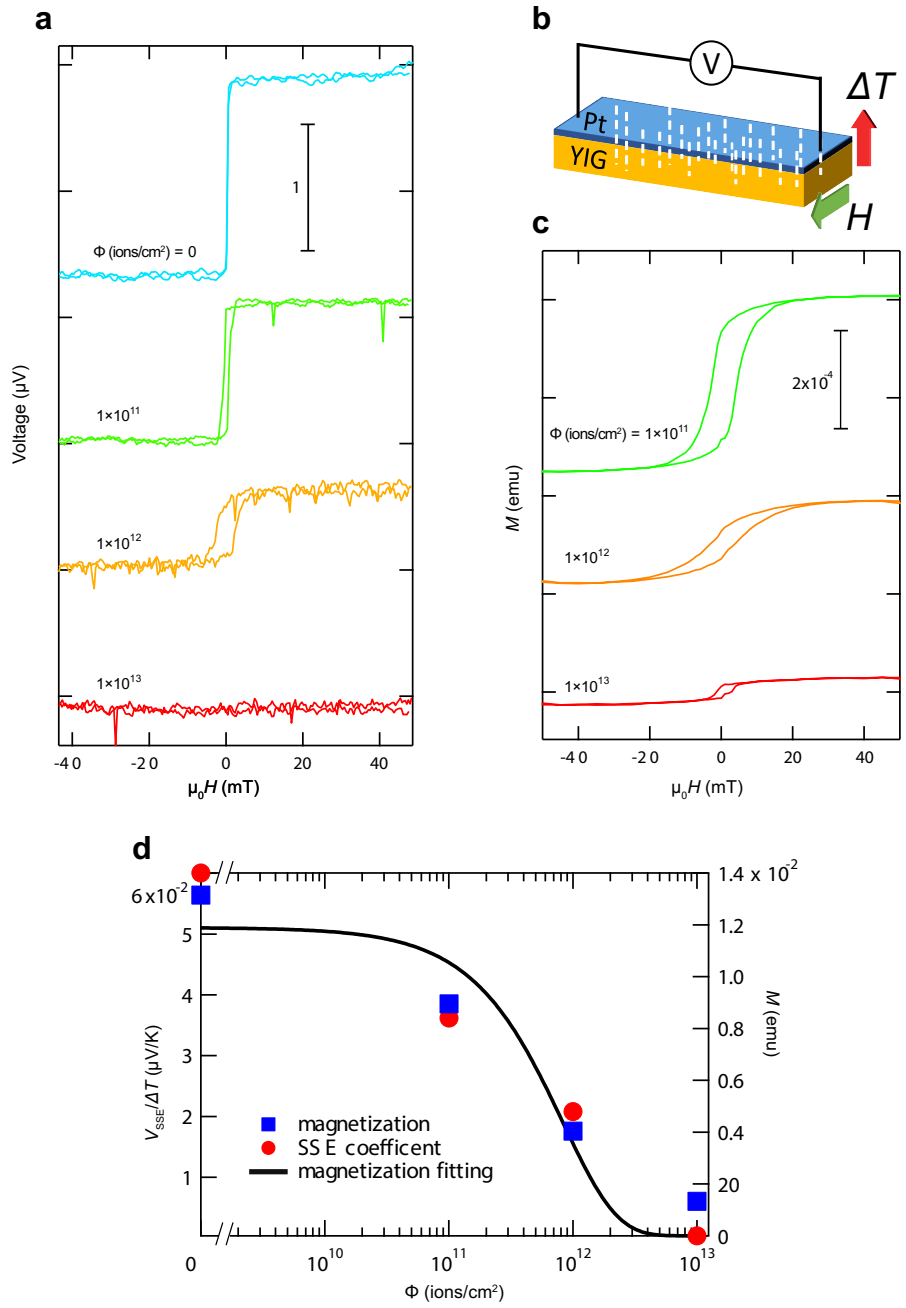
a
b
c
d
Voltage (μV)
Φ (ions/cm²) = 0
1×10¹¹
1×10¹²
1×10¹³
1
-40
-20
0
20
40
μ₀H (mT)
V
ΔT
Pt
YIG
H
M (emu)
2x10⁴
Φ (ions/cm²) = 1×10¹¹
1×10¹²
1×10¹³
μ₀H (mT)
6x10⁻²
1.4 x 10⁻²
V_SSE/ΔT (μV/K)
M (emu)
magnetization
SS E coefficent
magnetization fitting
10¹⁰
10¹¹
10¹²
10¹³
Φ (ions/cm²)

Figure 3

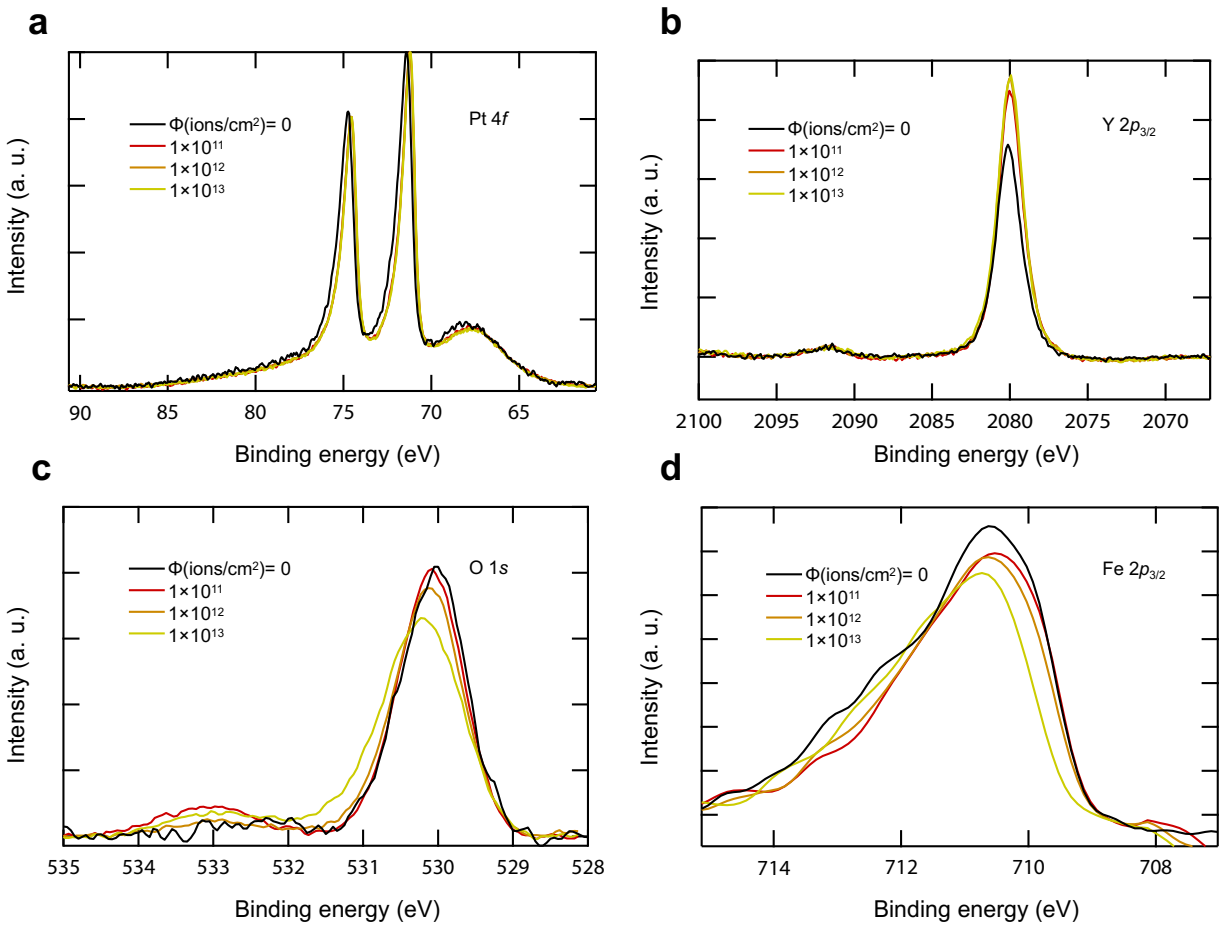
a
Φ(ions/cm²)= 0
1×10¹¹
1×10¹²
1×10¹³
Pt 4f
Intensity (a. u.)
90
85
80
75
70
65
Binding energy (eV)
b
Φ(ions/cm²)= 0
1×10¹¹
1×10¹²
1×10¹³
Y 2p3/2
Intensity (a. u.)
2100
2095
2090
2085
2080
2075
2070
Binding energy (eV)
c
Φ(ions/cm²)= 0
1×10¹¹
1×10¹²
1×10¹³
O 1s
Intensity (a. u.)
535
534
533
532
531
530
529
528
Binding energy (eV)
d
Φ(ions/cm²)= 0
1×10¹¹
1×10¹²
1×10¹³
Fe 2p3/2
Intensity (a. u.)
714
712
710
708
Binding energy (eV)